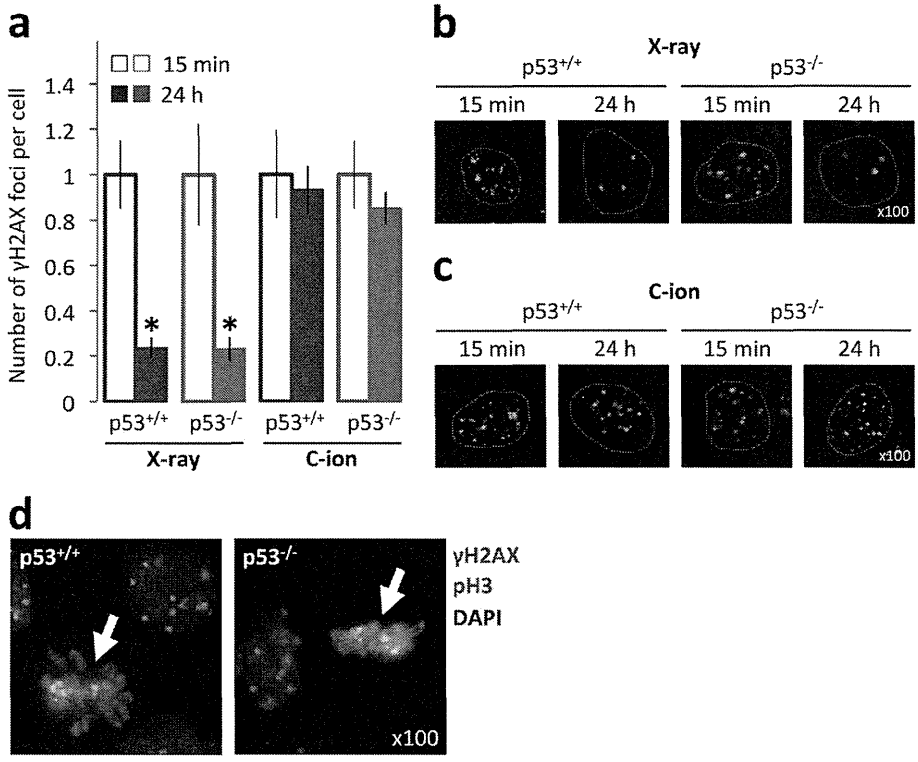

Fig. 7. Kinetics of DNA double-strand break generation by X-ray or carbon-ion beam irradiation in $p53^{+/+}$ and $p53^{-/-}$ HCT116 cells. Cells were seeded on glass coverslips, incubated overnight, exposed to X-rays (2 Gy) or carbon-ion beams (1 Gy), incubated for an additional 15 min or 24 h, and then subjected to immunostaining for γH2AX and pH3. Cells were then stained with DAPI. (a) Numbers of γH2AX foci per cell at 15 min or 24 h post-irradiation. The results for each cell line were normalized to the number of γH2AX foci at the 15 min time point. At least 500 cells were counted per experimental condition. Data are expressed as the mean ± SD. *$P<0.05$ versus the corresponding samples at 15 min. (b, c) Representative microscopic images showing nuclei exposed to X-ray (b) or carbon-ion beam (c) irradiation, and immunostained for γH2AX. In each panel, the outline of the nucleus detected by DAPI staining is indicated by a dashed line. (d) Representative microscopic images of nuclei exposed to carbon-ion beam irradiation and immunostained for γH2AX and pH 3 at 24 h post-irradiation. The arrows indicate double-positive nuclei. C-ion, carbon-ion.

doi:10.1371/journal.pone.0115121.g007

phase accumulation is the result of a defect in the p53-p21 signaling pathway that attenuates G1 arrest after irradiation [16]. This property of p53-deficient cancer cells might increase the chance of irradiated cells harboring unrepaired DSBs entering mitosis, leading to the enhancement of mitotic catastrophe.

The results of the present study suggest that both a lack of p53 and missense mutations in p53 contribute to the switch from apoptosis to mitotic catastrophe. Overall, 75% of the p53 mutations identified in human cancers are single missense mutations. Most missense mutations, including those examined in the present study, are located within the p53 DNA-binding domain, which plays a key role in the transcriptional activation of many target genes, including those that induce apoptosis [25]. Most mutant p53 proteins have a dominant-negative effect, leading to the dysfunction of the remaining normal p53 proteins. Therefore, it is reasonable that, along with the lack of p53, missense mutations in the p53 DNA-

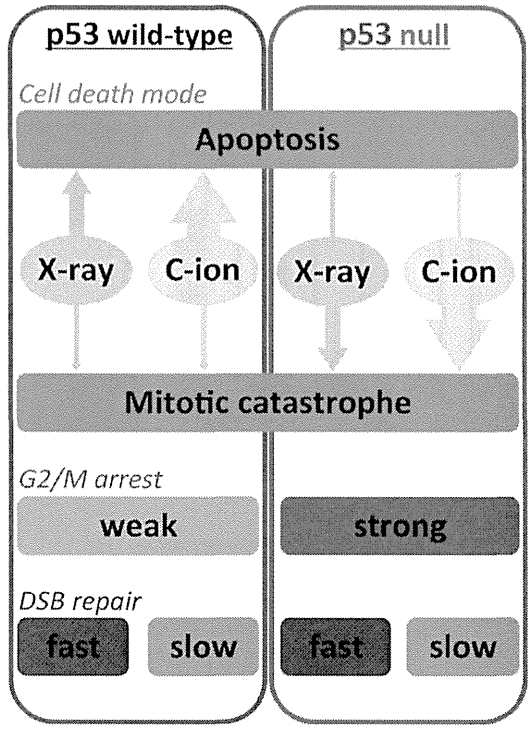

Fig. 8. Schematic model outlining the DNA damage response and cell death modes in p53 wild-type and -null cells after X-ray or carbon-ion beam irradiation. C-ion, carbon-ion.

doi:10.1371/journal.pone.0115121.g008

binding domain also contribute to the apoptosis-resistant phenotype by disrupting the ability of normal p53 proteins to transcriptionally activate apoptosis-related genes; this may render irradiated cells harboring unrepaired DSBs more susceptible to mitotic catastrophe. Nevertheless, it is worth noting a study limitation at this point: we were not able to establish H1299 cells expressing wild-type p53 (either transiently or stably); therefore, a comparison between wild-type p53 and mutant p53 was impossible. Future studies should compare the mode of irradiation-induced cell death in isogenic cell lines harboring wild-type, mutant, and null-p53.

Of note, the results presented here demonstrate efficient induction of mitotic catastrophe by carbon-ion beam irradiation in p53-null and p53-mutant cells. In fact, in all the p53-null and p53-mutant cells lines tested, the dose that are required to induce certain level of mitotic catastrophe was evidently lower in carbon-ion beams than in X-rays. This result can be explained by the difficulties associated with the repair of DSBs generated by carbon-ion beam irradiation, which retain more complex structures of damaged DNA ends than those generated by X-ray irradiation [35]. Inefficient DNA damage repair caused by the complexity of the DSB ends may underlie the efficient cell-killing effect of carbon-ion beam irradiation on cancer cells harboring p53 aberrations.

The results described here are partially contradictory to those of previous studies that examined the DDR after carbon-ion beam irradiation of p53-mutant cancer cells. Although a few studies observed efficient apoptosis (S2 Table) [12–15], it should be noticed that this mode of cell death was only induced efficiently at LET values greater than 70 keV/μm. By contrast, the average LET value at the center of the clinically-used spread-out Bragg peak, as used here, is approximately 50 keV/μm. In addition, in contrast to the results described here, the induction of senescence and prolonged (longer than 3 days) G2/M arrest was also observed in previous studies using carbon-ion beam irradiation with high LET values [12, 36]. These data suggest that the DDR differs depending on the LET value of the carbon-ion beam irradiation used. Additional *in vitro* and *in vivo* studies of a variety of cell lines are required to validate the therapeutic effects of carbon-ion beam irradiation at the LET used in clinical settings.

In summary, this comprehensive analysis of the DDR in irradiated isogenic cell lines demonstrates that X-ray irradiation-resistant p53-null cancer cells are susceptible to carbon-ion beam irradiation, which efficiently induces mitotic catastrophe (Fig. 8). The induction of mitotic catastrophe in apoptosis-resistant tumors may be an important biological advantage of carbon-ion radiotherapy over X-ray radiotherapy. Additional studies using animal models or clinical samples are required to elucidate this issue further.

Supporting Information

S1 Fig. Properties of the $p53^{+/+}$ and $p53^{-/-}$ cells.
doi:10.1371/journal.pone.0115121.s001 (PDF)

S2 Fig. The modes of cell death induced by X-ray irradiation for the D_{10} in HCT116 $p53^{-/-}$ cells.
doi:10.1371/journal.pone.0115121.s002 (PDF)

S3 Fig. The modes of cell death induced by X-ray or carbon-ion beam irradiation in BJ hTERT-WT or -shp53 cells.
doi:10.1371/journal.pone.0115121.s003 (PDF)

S1 Table. The number of γH2AX foci per cell after irradiation.
doi:10.1371/journal.pone.0115121.s004 (PDF)

S2 Table. LET-dependency of the efficacy of apoptosis induction by carbon-ion beam irradiation in p53-mutant cancer cells.
doi:10.1371/journal.pone.0115121.s005 (PDF)

Acknowledgments

We thank Dr. Tetsushi Sadakata, Dr. Kohta Torikai, and Dr. Mayumi Komachi (Gunma University) for technical assistance. We thank Dr. Volgelstein (Johns Hopkins University) for providing cell lines.

Author Contributions

Conceived and designed the experiments: NA T. Oike AS HO MI YY T. Ohno TK TN. Performed the experiments: NA T. Oike NT MY YS RS. Analyzed the data: NA T. Oike AS HO TK. Contributed reagents/materials/analysis tools: NA T. Oike AS HO NT MY YS RS MI YY T. Ohno TK TN. Wrote the paper: NA T. Oike AS.

References

1. **Schulz-Ertner D, Tsujii H** (2007) Particle radiation therapy using proton and heavier ion beams. J Clin Oncol 25: 953–964.
2. **Loeffler JS, Durante M** (2013) Charged particle therapy—optimization, challenges and future directions. Nat Rev Clin Oncol 10: 411–424.
3. **Yamada S** (2014) Postoperative Recurrence of Rectal Cancer. In: Tsujii H, Kamada T, Shirai T, Noda K, Tsuji H, Karasawa K, editors. Carbon-Ion Radiotherapy: Principles, Practices, and Treatment Planning. Tokyo: Springer. pp. 203–209.
4. **Ciatto S, Pacini P** (1982) Radiation therapy for recurrences of carcinoma of the rectum and sigmoid after surgery. Acta Radiol Oncol 21: 105–109.
5. **Mak RH, Doran E, Muzikansky A, Kang J, Neal JW, et al.** (2011) Outcomes after combined modality therapy for EGFR-mutant and wild-type locally advanced NSCLC. Oncologist 16: 886–895.
6. **Torres-Roca JF** (2012) A molecular assay of tumor radiosensitivity: a roadmap towards biology-based personalized radiation therapy. Per Med 9: 547–557.
7. **Ishikawa H, Mitsuhashi N, Sakurai H, Maebayashi K, Niibe H** (2001) The effects of P53 status and human papillomavirus infection on the clinical outcome of patients with stage IIIB cervical carcinoma treated with radiation therapy alone. Cancer 91: 80–89.
8. **Huerta S, Hrom J, Gao X, Saha D, Anthony T, et al.** (2010) Tissue microarray constructs to predict a response to chemoradiation in rectal cancer. Dig Liver Dis 42: 679–684.
9. **Giono LE, Manfredi JJ** (2006) The p53 tumor suppressor participates in multiple cell cycle checkpoints. J Cell Physiol 209: 13–20.
10. **Takahashi T, Fukawa T, Hirayama R, Yoshida Y, Musha A, et al.** (2010) In vitro interaction of high-LET heavy-ion irradiation and chemotherapeutic agents in two cell lines with different radiosensitivities and different p53 status. Anticancer Res 30: 1961–1967.
11. **Huerta S, Gao X, Dineen S, Kapur P, Saha D, et al.** (2013) Role of p53, Bax, p21, and DNA-PKcs in radiation sensitivity of HCT-116 cells and xenografts. Surgery 154: 143–151.
12. **Maalouf M, Alphonse G, Colliaux A, Beuve M, Trajkovic-Bodennec S, et al.** (2009) Different mechanisms of cell death in radiosensitive and radioresistant p53 mutated head and neck squamous cell carcinoma cell lines exposed to carbon-ions and x-rays. Int J Radiat Oncol Biol Phys 74: 200–209.
13. **Yamakawa N, Takahashi A, Mori E, Imai Y, Furusawa Y, et al.** (2008) High LET radiation enhances apoptosis in mutated p53 cancer cells though Caspase-9 activation. Cancer Sci 99: 1455–1460.
14. **Takahashi A, Matsumoto H, Yuki K, Yasumoto J, Kajiwara A, et al.** (2004) High-LET radiation enhanced apoptosis but not necrosis regardless of p53 status. Int J Radiat Oncol Biol Phys 60: 591–597.
15. **Takahashi A, Ohnishi K, Ota I, Asakawa I, Tomamoto T, et al.** (2001) p53-dependent thermal enhancement of cellular sensitivity in human spuamous cell carcinomas in relation to LET. Int J Radiat Biol 77: 1043–1051.
16. **Bunz F, Dutriaux A, Lengauer C, Waldman T, Zhou S, et al.** (1998) Requirement for p53 and p21 to sustain G2 arrest after DNA damage. Science 282: 1497–1501.
17. **Kurioka D, Takeshita F, Tsuta K, Sakamoto H, Watanabe S, et al.** (2014) NEK9-dependent proliferation of cancer cells lacking functional p53. Sci Rep 4: 6111.

18. **Yamauchi M, Suzuki K, Oka Y, Suzuki M, Kondo H, et al.** (2011) Mode of ATM-dependent suppression of chromosome translocation. Biochem Biophys Res Commun 416: 111–108.

19. **Oike T, Ogiwara H, Torikai K, Nakano T, Yokota J, et al.** (2012) Garcinol, a histone acetyltransferase inhibitor, radiosensitizes cancer cells by inhibiting non-homologous end joining. Int J Radiat Oncol Biol Phys 84: 815–821.

20. **Oike T, Ogiwara H, Tominaga Y, Ito K, Ando O, et al.** (2013) A synthetic lethality-based strategy to treat cancers harboring a genetic deficiency in the chromatin remodeling factor BRG1. Cancer Res 73: 5508–5518.

21. **Sawai Y, Murata H, Horii M, Koto K, Matsui T, et al.** (2013) Effectiveness of sulforaphane as a radiosensitizer for murine osteosarcoma cells. Oncol Rep 29: 941–945.

22. **Russo AL, Kwon HC, Burgan WE, Carter D, Beam K, et al.** (2009) In vitro and in vivo radiosensitization of glioblastoma cells by the poly (ADP-ribose) polymerase inhibitor E7016. Clin Cancer Res 15: 607–612.

23. **Di Micco R, Sulli G, Dobreva M, Liontos M, Botrugno OA, et al.** (2011) Interplay between oncogene-induced DNA damage response and heterochromatin in senescence and cancer. Nat Cell Biol 13: 292–302.

24. **Nakajima NI, Brunton H, Watanabe R, Shrikhande A, Hirayama R, et al.** (2013) Visualisation of γH2AX foci caused by heavy ion particle traversal; distinction between core track versus non-track damage. PLoS One 8: e70107.

25. **Bullock AN, Fersht AR** (2001) Rescuing the function of mutant p53. Nat Rev Cancer 1: 68–76.

26. **Wouters BG** (2009) Cell death after irradiation: how, when and why cells die. In: Joiner M and van der Kogel A, editors. Basic Clinical Radiobiology. 4th ed. London: Hodder Education. pp. 27–40.

27. **Hall EJ, Giaccia AJ** (2006) DNA strand breaks and chromosomal aberrations. In: McAllister L ed. Radiobiology for the radiologist. 6th ed. Philadelphia: Lippincott Williams & Wilkins. pp. 16–29.

28. **Lobrich M, Shibata A, Beucher A, Fisher A, Ensminger M, et al.** (2010) γH2AX foci analysis for monitoring DNA double-strand break repair: Strengths, limitations and optimization. Cell Cycle 9: 662–669.

29. **Shibata A, Conrad S, Birraux J, Geuting V, Barton O, et al.** (2011) Factors determining DNA double-strand break repair pathway choice in G2 phase. EMBO J 30: 1079–1092.

30. **Bucher N and Britten CD** (2008) G2 checkpoint abrogation and checkpoint kinase-1 targeting in the treatment of cancer. Br J Cancer 98: 523–528.

31. **Deckbar D, Jeggo PA, Lobrich M** (2011) Understanding the limitations of radiation-induced cell cycle checkpoints. Crit Rev Biochem Mol Biol 46: 271–283.

32. **Lukas C, Savic V, Bekker-Jensen S, Doil C, Neumann B, et al.** (2011) 53BP1 nuclear bodies form around DNA lesions generated by mitotic transmission of chromosomes under replication stress. Nat Cell Biol 13: 243–253.

33. **Harrigan JA, Belotserkovskaya R, Coates J, Dimitrova DS, Polo SE, et al.** (2011) Replication stress induces 53BP1-containing OPT domains in G1 cells. J Cell Biol 193: 97–108.

34. **Giunta S, Belotserkovskaya R, Jackson SP** (2010) DNA damage signaling in response to double-strand breaks during mitosis. J Cell Biol 190: 197–207.

35. **Terato H, Ide H** (2004) Clustered DNA damage induced by heavy ion particles. Biol Sci Space 18: 206–215.

36. **Oishi T, Sasaki A, Hamada N, Ishiuchi S, Funayama T, et al.** (2008) Proliferation and cell death of human glioblastoma cells after carbon-ion beam exposure: Morphologic and morphometric analyses. Neuropathology 28: 408–416.

Journal of Radiation Research Advance Access published January 18, 2015

Journal of Radiation Research, 2015, pp 1–10
doi: 10.1093/jrr/rru085

Regular Paper

Radiosensitizing effect of carboplatin and paclitaxel to carbon-ion beam irradiation in the non-small-cell lung cancer cell line H460

Nobuteru KUBO[1], Shin-ei NODA[1,*], Akihisa TAKAHASHI[2], Yukari YOSHIDA[3], Takahiro OIKE[1], Kazutoshi MURATA[1], Atsushi MUSHA[3], Yoshiyuki SUZUKI[1], Tatsuya OHNO[3], Takeo TAKAHASHI[4] and Takashi NAKANO[1,3]

[1]Department of Radiation Oncology, Gunma University Graduate School of Medicine, 3-39-22 Showa-machi, Maebashi, Gunma, 371-8511, Japan
[2]Advanced Scientific Research Leaders Development Unit, Gunma University, Gunma, Japan
[3]Gunma University Heavy Ion Medical Center, Gunma, Japan
[4]Department of Radiology, Saitama Medical Center, Saitama Medical University, Saitama, Japan
*Corresponding author. Department of Radiation Oncology, Gunma University Graduate School of Medicine, 3-39-22 Showa-machi, Maebashi, Gunma, 371-8511, Japan. Tel: +81-27-220-8383; Fax: +81-27-220-8397;
Email: snoda@gunma-u.ac.jp

(Received 24 May 2014; revised 22 August 2014; accepted 27 August 2014)

The present study investigated the ability of carboplatin and paclitaxel to sensitize human non-small-cell lung cancer (NSCLC) cells to carbon-ion beam irradiation. NSCLC H460 cells treated with carboplatin or paclitaxel were irradiated with X-rays or carbon-ion beams, and radiosensitivity was evaluated by clonogenic survival assay. Cell proliferation was determined by counting the number of viable cells using Trypan blue. Apoptosis and senescence were evaluated by terminal deoxynucleotidyl transferase-mediated dUTP nick-end labeling (TUNEL) staining and senescence-associated β-galactosidase (SA-β-gal) staining, respectively. The expression of cleaved caspase-3, Bax, p53 and p21 was analyzed by western blotting. Clonogenic survival assays demonstrated a synergistic radiosensitizing effect of carboplatin and paclitaxel with carbon-ion beams; the sensitizer enhancement ratios (SERs) at the dose giving a 10% survival fraction (D_{10}) were 1.21 and 1.22, respectively. Similarly, carboplatin and paclitaxel showed a radiosensitizing effect with X-rays; the SERs were 1.41 and 1.29, respectively. Cell proliferation assays validated the radiosensitizing effect of carboplatin and paclitaxel with both carbon-ion beam and X-ray irradiation. Carboplatin and paclitaxel treatment combined with carbon-ion beams increased TUNEL-positive cells and the expression of cleaved caspase-3 and Bax, indicating the enhancement of apoptosis. The combined treatment also increased SA-β-gal-positive cells and the expression of p53 and p21, indicating the enhancement of senescence. In summary, carboplatin and paclitaxel radiosensitized H460 cells to carbon-ion beam irradiation by enhancing irradiation-induced apoptosis and senescence.

Keywords: carbon-ion beams; lung cancer; radiosensitization; paclitaxel; carboplatin

INTRODUCTION

The standard treatment for patients with unresectable locally advanced non-small-cell lung cancer (NSCLC) is combined treatment with radiotherapy and chemotherapy. In the combined treatment, radiotherapy plays a local role by targeting the primary disease site. Meanwhile, chemotherapy serves as a radiosensitizer to increase the intensity of local therapy, and also functions as a systemic therapy targeting micrometastasis throughout the body. To date, the clinical outcome from chemoradiotherapy for locally advanced NSCLC is far from satisfactory because the 5-year overall survival rate is 15–20%. Importantly, in this population, the local recurrence rate accounts for ~30% of patients [1–3], highlighting the necessity of increasing the efficacy of local therapy. To this end, X-ray dose-escalation studies have been conducted for locally advanced NSCLC; however, they have not resulted in significant clinical benefit [4, 5]. The limitation of the X-ray

dose-escalation strategy in locally advanced NSCLC is attributed to the characteristics of the dose distribution achieved by X-rays; i.e. the curative dose cannot be delivered to tumors without exceeding the tolerance of the surrounding organs. Therefore, an alternative method of improving the efficacy of local therapy for locally advanced NSCLC is required.

Recently, carbon-ion beam radiotherapy has generated a great deal of interest as a highly intensive local therapy. Carbon-ion beams have a Bragg peak that results in distal tail-off and a sharp penumbra [6]. This property of carbon-ion beams allows for a highly conformal dose distribution, such that a high dose can be delivered to tumors while maintaining a tolerable dose in the surrounding normal organs, resulting in highly intensive radiotherapy. In early NSCLC, carbon-ion beam radiotherapy has shown a 5-year local control rate of 90–95%, indicating that it can be applied to locally advanced NSCLC. However, of note, subgroup analysis has also shown that the local recurrence rate is negatively correlated with the diameter of the tumors (i.e. T2 tumors versus T1 tumors) [7, 8], suggesting that further enhancement of carbon-ion beam radiotherapy is required to control the primary disease site in locally advanced NSCLC cases.

The addition of chemotherapeutic drugs to carbon-ion radiotherapy could be a possible way to enhance its efficacy. A radiosensitizing effect of various chemotherapeutic drugs to carbon-ion beam irradiation has been shown in various human cancer types *in vitro*, e.g. docetaxel in esophageal cancer cells [9], temozolomide in glioblastoma cells [10], and camptothecin, cisplatin, gemcitabine and paclitaxel in colon cancer cells [11]. On the other hand, in X-ray chemoradiotherapy for locally advanced NSCLC, the standard chemotherapeutic regimen is the 'platinum-doublet', the combination of a platinum drug with a drug of a different class. One of the most common combinations of drugs in platinum-doublet chemotherapy is carboplatin and paclitaxel. Carboplatin is a platinum drug that generates intra- and inter-strand crosslinks in DNA [12], while paclitaxel is a microtubule-stabilizing agent that disturbs mitosis by suppressing spindle microtubule dynamics at metaphase [13]. In the clinical setting of X-ray radiotherapy, concomitant chemoradiotherapy using carboplatin plus paclitaxel has shown favorable outcomes [14, 15] compared with radiotherapy alone [4, 16]. In fact, there have been no clinical studies directly comparing chemoradiotherapy using carboplatin plus paclitaxel with radiotherapy alone. Nevertheless, comparison of the outcomes of Phase II and III clinical trials demonstrates that the median survival of chemoradiotherapy using carboplatin plus paclitaxel (22.0–26.9 months) is superior to that of radiotherapy alone (9.7–11.4 months). These data suggest that carboplatin and paclitaxel could be applied to combination use with carbon-ion beam radiotherapy to improve the efficacy of carbon-ion beam radiotherapy in locally advanced NSCLC; however, the combined effect of carboplatin or paclitaxel with carbon-ion beam irradiation in NSCLC cells has not been investigated. In the present study, to provide a biological basis for the combined use of carboplatin and paclitaxel with carbon-ion beam radiotherapy, we investigated the ability of carboplatin and paclitaxel to sensitize a human NSCLC cell line to carbon-ion beam irradiation *in vitro*.

MATERIALS AND METHODS

Cell line

The human NSCLC cell line H460 was obtained from the American Type Culture Collection (Manassas, VA). Cells were cultured at 37°C in a humidified 5% CO_2 atmosphere in RPMI-1640 medium supplemented with 10% FBS, 100 U/ml penicillin and 100 μg/ml streptomycin (Life Technologies, Carlsbad, CA).

Irradiation

Carbon-ion beam irradiation (290 MeV/nucleon) was performed at Gunma University Heavy Ion Medical Center (Gunma, Japan) [17]. Cells cultured on 60-mm dishes were irradiated with carbon-ion beams at the center of a 6-cm spread-out Bragg peak (SOBP) in the vertical direction. The linear energy transfer (LET) at the center of the SOBP was ~50 keV/μm.

X-ray irradiation was performed using a Faxitron RX-650 (Faxitron Bioptics, LCC, Tucson, AZ) operated at 100 kVp with a dose rate of 1.14 Gy/min.

Chemotherapeutic drugs

Carboplatin and paclitaxel (Wako Pure Chemical Industries, Tokyo, Japan) were solubilized in dimethyl sulfoxide (DMSO) and prepared as stock solutions at 100 mM and 1 mM, respectively. The drugs were diluted to their final concentrations with culture medium, resulting in a DMSO concentration of less than 0.01% by weight/volume. Therefore, DMSO was not added to the control samples.

Treatments

Cells were plated on culture dishes in media containing carboplatin or paclitaxel for 24 h. The drug-containing media was replaced with drug-free media immediately prior to irradiation with X-rays or carbon-ion beams.

Clonogenic survival assay

Nine days after irradiation, cells were fixed with 100% ethanol and stained with 2% crystal violet. Colonies consisting of >50 cells were counted. The plating efficiency of untreated cells was 83.3 ± 7.7%. The surviving fractions of cells treated with irradiation plus a single drug were normalized to the surviving fractions of cells treated with that drug alone. Survival curves were obtained by fitting the surviving fractions to a linear–quadratic model expressed by the following formula: $SF = \exp - (\alpha D + \beta D^2)$, where SF is the surviving fraction and

D is the dose. The dose resulting in a surviving fraction of 10% (D_{10}) was calculated from the survival curves. The relative biological effectiveness (RBE) of carbon-ion beams compared with X-rays was calculated at the D_{10}. The sensitizer enhancement ratio (SER), an indicator of the radiosensitizing effect of a drug of interest, was calculated as the ratio of the D_{10} of cells treated with irradiation alone to the D_{10} of cells treated with irradiation plus the drug.

Cell proliferation assay

Three days after irradiation, the cells were harvested and centrifuged. The pellets were resuspended in PBS containing Trypan blue (Bio-Rad Laboratories, Tokyo, Japan). Viable cells negative for Trypan blue staining [18] were counted using a TC20 Automated Cell Counter (Bio-Rad Laboratories). Cell proliferation was calculated as the ratio of the number of viable cells in the treated group to that in the untreated control group.

TUNEL staining

Apoptosis was evaluated by terminal deoxynucleotidyl transferase-mediated dUTP nick-end labeling (TUNEL) staining using the ApopTag Fluorescein *In Situ* Apoptosis Detection Kit S7100 (Millipore, Billerica, MA). Three days after irradiation, cells were subjected to dual staining with TUNEL and 4,6-diamino-2-phenylindole (DAPI) (Life Technologies) according to the manufacturer's protocol. TUNEL staining positivity was calculated as the ratio of the number of cells positive for TUNEL staining to the number of cells positive for DAPI staining. For each experimental condition, at least 300 cells were scored.

Senescence-associated β-galactosidase staining

Senescence was evaluated by senescence-associated β-galactosidase (SA-β-gal) staining using the Senescence β-Galactosidase Staining Kit (Cell Signaling Technology, Tokyo, Japan) according to the manufacturer's instructions. Three days after irradiation, cells were subjected to SA-β-gal staining. Senescent cells were identified (by blue staining under light microscopy) and counted. For each experimental condition, at least 300 cells were scored.

Western blotting

Three days after irradiation, cells were harvested, lysed with Cell Lysis Buffer (Millipore) containing phosphatase inhibitor cocktails 1 and 2 (Sigma–Aldrich, St Louis, MO) and protease inhibitor cocktail 3 (Calbiochem, San Diego, CA), and centrifuged at 15 000 g. Protein concentrations of the lysates were determined using the BCA Protein Assay Kit (Pierce, Rockford, IL) and the samples were subjected to western blot analysis. The samples were resolved by SDS-polyacrylamide gel electrophoresis and transferred to PVDF membranes. Bax, p53, p21 and cleaved caspase-3 (Asp175) were evaluated using the corresponding primary antibodies (Cell Signaling Technology, Danvers, MA). Actin (Sigma–Aldrich) was used as a loading control. The primary antibodies were labeled with a horseradish peroxidase-conjugated secondary antibody, and the proteins were visualized using the electrochemiluminescent detection system (GE Healthcare, Tokyo, Japan).

Statistics

The data from three independent experiments were expressed as the mean values with standard deviations (SDs). Statistical significance was determined by Student's *t*-test using IBM SPSS Statistics 21.0 software (IBM, Armonk, NY). A P-value < 0.05 was considered to be statistically significant.

RESULTS

Radiosensitizing effect of carboplatin and paclitaxel to carbon-ion beams

The cytotoxicity of carboplatin and paclitaxel in H460 cells was assessed by clonogenic survival assay (Fig. 1), and both drugs showed a dose-responsive relationship to survival. The median effective doses (IC_{50}) of carboplatin and paclitaxel were 7.9 μM and 8.3 nM, respectively; these IC_{50} values were employed in subsequent experiments, based on previous studies investigating the radiosensitizing effects of chemotherapeutic drugs [9, 11].

The survival of H460 cells irradiated with X-rays or carbon-ion beams was assessed by clonogenic survival assay (Fig. 2). The RBE of carbon-ion beams to X-rays was calculated as 2.3. Both carboplatin and paclitaxel showed a radiosensitizing effect to X-rays (Fig. 2A) and carbon-ion beam irradiation (Fig. 2B). The SER of carboplatin was 1.41 for X-ray irradiation and 1.21 for carbon-ion beam irradiation, which was significantly higher for X-rays than for carbon-ion beams ($P = 0.03$) (Table 1). The SER of paclitaxel was 1.29 for X-ray and 1.22 for carbon-ion beam irradiation, which was not a significant difference ($P = 0.09$) (Table 1).

Effects of carboplatin and paclitaxel on proliferation of cells irradiated by carbon-ion beams

Next, a cell proliferation assay was performed to validate the radiosensitizing effect that was observed in the clonogenic survival assay (Fig. 3). As expected, at a dose of 4 Gy, carbon-ion beam irradiation suppressed cell proliferation more effectively than X-ray irradiation (18.9% vs 56.1%, $P < 0.001$). The experiment was next repeated using the iso-survival doses obtained from the clonogenic survival assay (i.e. 9 Gy with X-ray and 4 Gy with carbon-ion beams, which resulted in survival fractions of 4.6% and 4.5%, respectively) (Fig. 1). Irradiation with X-rays or carbon-ion beams at these doses suppressed cell proliferation to a similar extent (17.3% with X-ray and 18.9% with carbon-ion beams; $P = 0.57$), which was consistent with the results of the clonogenic survival assay. At the iso-survival doses, the addition of carboplatin significantly reduced the

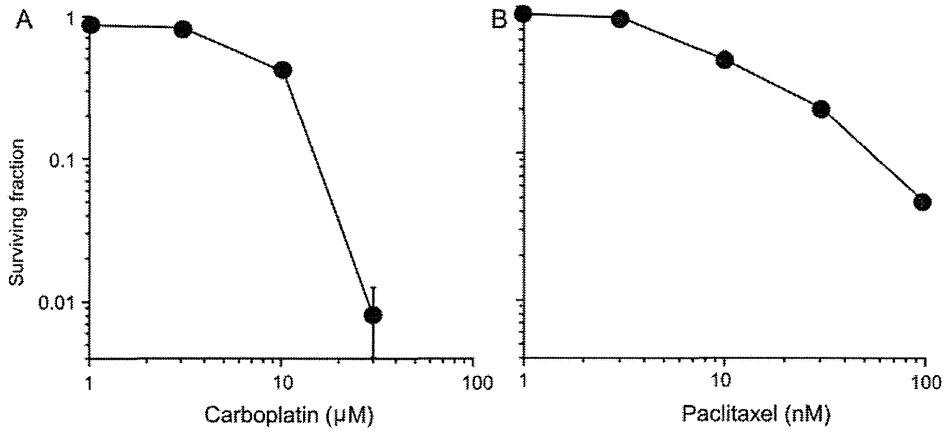

Fig. 1. Cytotoxicity of carboplatin and paclitaxel in H460 cells assessed by clonogenic survival assay. (**A**) Carboplatin. (**B**) Paclitaxel. The mean ± SD is shown.

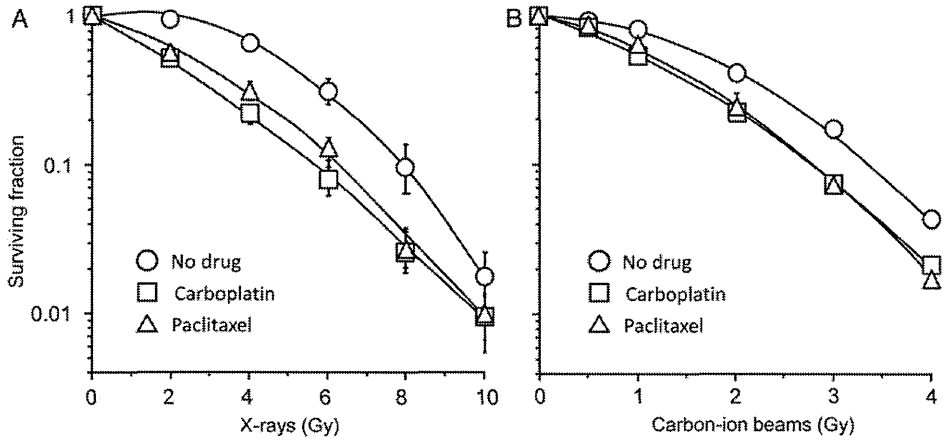

Fig. 2. Effects of carboplatin and paclitaxel on the survival of H460 cells irradiated with X-rays or carbon-ion beams. Survival curves of cells receiving X-ray (**A**) and carbon-ion beam (**B**) irradiation. Carboplatin and paclitaxel were used at each respective IC_{50} (7.9 μM and 8.3 nM). Datapoints were fitted to the linear–quadratic model. The mean ± SD is shown.

Table 1. D_{10} values from clonogenic assays and calculated sensitizer enhancement ratios

	X-rays			Carbon-ion beams		
	No drug	**CBDCA**	**PTX**	**No drug**	**CBDCA**	**PTX**
D_{10} (Gy)	7.99 ± 0.40	5.68 ± 0.40	6.20 ± 0.21	3.42 ± 0.07	2.82 ± 0.05	2.82 ± 0.08
SER		1.41 ± 0.10 ($P = 0.003$)	1.29 ± 0.04 ($P = 0.002$)		1.21 ± 0.02 ($P < 0.001$)	1.22 ± 0.04 ($P < 0.001$)

D_{10} = the dose leading to a survival rate of 10%, CBDCA = carboplatin, PTX = paclitaxel, SER = sensitizer enhancement ratio.

proliferation of cells irradiated with either X-ray or carbon-ion beams (10.1% and 9.8%, respectively) compared with cells treated with irradiation alone. The radiosensitizing effect of carboplatin was comparable between X-rays and carbon-ion beams ($P = 0.87$). Similarly, at the iso-survival doses, the addition of paclitaxel significantly reduced the proliferation of cells irradiated with either X-ray or carbon-ion beams (6.3% and 6.4%, respectively) compared with cells treated with irradiation alone. The radiosensitizing effect of paclitaxel was also comparable between X-ray and carbon-ion beams ($P = 0.95$). These data validated the radiosensitizing effect of carboplatin and paclitaxel to both X-ray and carbon-ion beam irradiation.

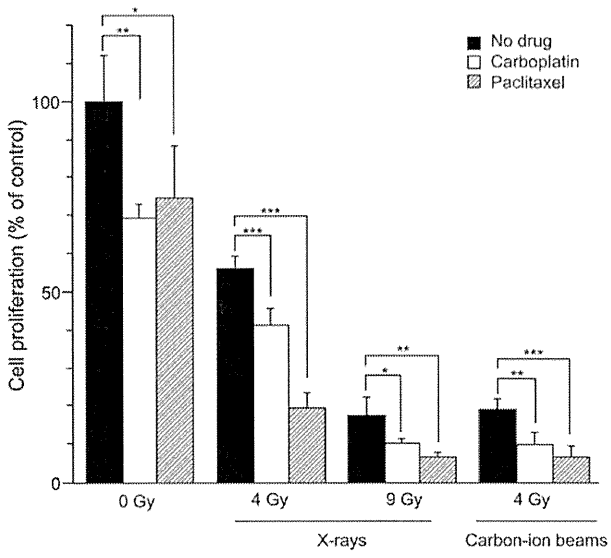

Fig. 3. Effects of carboplatin and paclitaxel on the inhibition of H460 cell proliferation by X-ray or carbon-ion beam irradiation. Cell proliferation was calculated as the ratio of the number of viable cells in a treated group to that in the untreated control group 3 days after irradiation. Viable cells were determined by negativity for Trypan blue. Carboplatin and paclitaxel were used at each respective IC_{50} (7.9 μM and 8.3 nM). The mean ± SD is shown. A single asterisk indicates $P < 0.05$; two asterisks indicate $P < 0.01$; three asterisks indicate $P < 0.001$.

Carboplatin and paclitaxel enhanced apoptosis induced by carbon-ion beam irradiation

Next, TUNEL staining was used to determine whether the induction of apoptosis was enhanced by carboplatin or paclitaxel in cells irradiated with X-rays or carbon-ion beams (Fig. 4). A representative micrograph of apoptotic cells is shown in Fig. 4A. X-ray irradiation induced apoptosis in a dose-dependent manner (0, 4 and 9 Gy) (Fig. 4B). At both 4 Gy and 9 Gy, the addition of carboplatin or paclitaxel significantly enhanced apoptosis in cells irradiated by X-rays. Carbon-ion beam irradiation at 4 Gy also induced apoptosis. At 4 Gy, the addition of carboplatin or paclitaxel significantly enhanced apoptosis in cells treated with carbon-ion beam irradiation. Irradiation by X-ray or carbon-ion beam at the iso-survival doses obtained from the clonogenic survival assay (Fig. 1) resulted in a comparable induction of apoptosis (4.5% with X-rays vs 3.2% with carbon-ion beams, $P = 0.07$). At the iso-survival doses, the additional effect of carboplatin or paclitaxel on the induction of apoptosis was comparable between X-rays and carbon-ion beams (2.5% for X-rays and carboplatin vs 2.6% for carbon-ion beams and carboplatin, $P = 0.82$; 3.5% for X-rays and paclitaxel vs 4.4% for carbon-ion beams and paclitaxel, $P = 0.30$).

The enhancement of apoptosis by carboplatin or paclitaxel in carbon-ion beam-irradiated cells was further investigated by western blotting. The addition of carboplatin or paclitaxel to cells irradiated with carbon-ion beams resulted in an increase in the expression of cleaved caspase-3 and Bax, which are involved in the activation of the apoptosis pathway [19, 20] (Fig. 4C). Together, these results indicate that carboplatin and paclitaxel enhanced apoptosis induced by carbon-ion beam irradiation.

Carboplatin and paclitaxel enhanced senescence induced by carbon-ion beam irradiation

Finally, SA-β-gal staining was used to examine whether the induction of senescence is enhanced by carboplatin or paclitaxel in cells irradiated with X-rays or carbon-ion beams (Fig. 5). A representative micrograph of senescent cells is shown in Fig. 5A. As shown in the right panel of Fig. 5A, senescent cells not only stained blue but also showed an enlarged and flattened morphology [21]. X-ray irradiation induced senescence in a dose-dependent manner (0, 4 and 9 Gy) (Fig. 5B). At 4 Gy and 9 Gy, the addition of carboplatin significantly enhanced senescence in cells irradiated by X-rays, and at 4 Gy, the addition of paclitaxel significantly enhanced senescence in cells irradiated by X-rays. Carbon-ion beam irradiation at 4 Gy also induced senescence. At 4 Gy, the addition of carboplatin or paclitaxel significantly enhanced senescence in carbon-ion beam-irradiated cells. Irradiation by X-ray or carbon-ion beam at the iso-survival doses obtained from the clonogenic survival assay (Fig. 1) resulted in a comparable induction of senescence (85.0% in cells irradiated by X-rays vs 82.2% in those irradiated by carbon-ion beams, $P = 0.52$). At the iso-survival doses, the additional effect of carboplatin or paclitaxel on the induction of senescence was comparable in cells irradiated by X-rays or carbon-ion beams (10.6% with X-rays and carboplatin vs 10.0% with carbon-ion beams and carboplatin, $P = 0.82$; 8.4% with X-rays and paclitaxel vs 11.3% with carbon-ion beams and paclitaxel, $P = 0.48$).

We further investigated the enhancement of senescence by carboplatin or paclitaxel in carbon-ion beam-irradiated cells by western blotting for p21 and p53, because p21 is involved in the induction of senescence and p53 is a positive regulator of p21 [22]. The addition of carboplatin or paclitaxel increased the expression of p21 and p53 in cells irradiated by carbon-ion beams (Fig. 5C). Together, these results indicate that carboplatin and paclitaxel enhanced the induction of senescence by carbon-ion beam irradiation.

DISCUSSION

The present study showed that carboplatin and paclitaxel sensitized NSCLC H460 cells to carbon-ion beam irradiation by enhancing irradiation-induced apoptosis and senescence.

The cytotoxic effect of ionizing irradiation is mainly based on the generation of DNA double-strand breaks (DSBs). When cells receive ionizing irradiation, DNA damage response

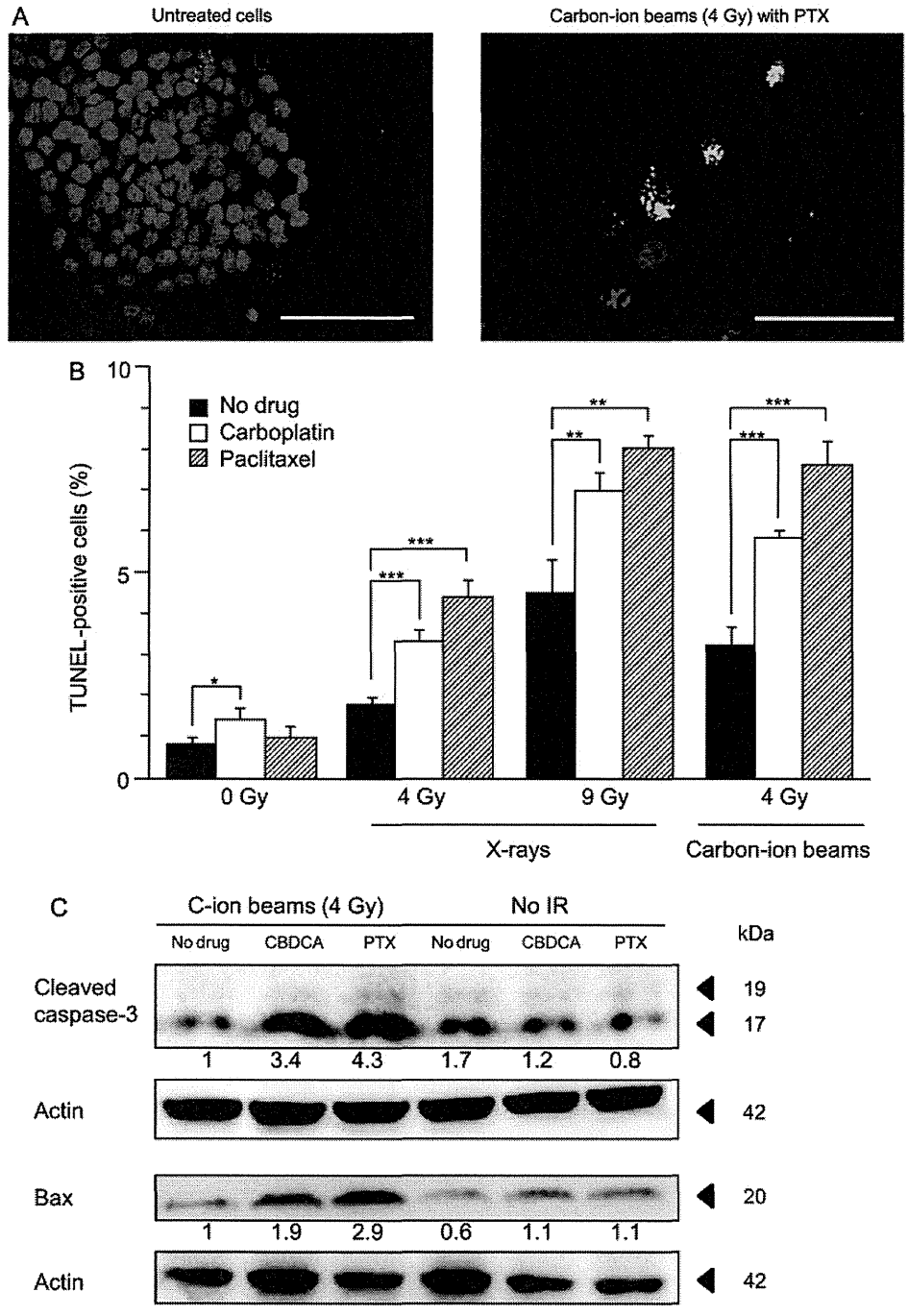

Fig. 4. Effects of carboplatin and paclitaxel on apoptosis induction in H460 cells irradiated with X-rays or carbon-ion beams. (**A**) Representative micrograph of cells negative (left panel) and positive (right panel) for terminal deoxynucleotidyl transferase-mediated dUTP nick-end labeling (TUNEL) staining. TUNEL and 4,6-diamino-2-phenylindole (DAPI) staining are shown by green and blue fluorescence, respectively. Bars, 100 μm. (**B**) Percentages of TUNEL-positive cells. The mean ± SD is shown. A single asterisk indicates $P < 0.05$; two asterisks indicate $P < 0.01$; three asterisks indicate $P < 0.001$. (**C**) Western blotting for cleaved caspase-3 and Bax. Actin was used as a loading control. Levels of cleaved caspase-3 and Bax are shown as ratios to their levels in cells treated with carbon-ion beam irradiation alone, after normalization to loading controls. TUNEL staining and Western blotting were performed 3 days after irradiation. Carboplatin and paclitaxel were used at each respective IC_{50} (7.9 μM and 8.3 nM). C-ion = carbon-ion, CBDCA = carboplatin, PTX = paclitaxel, IR = irradiation.

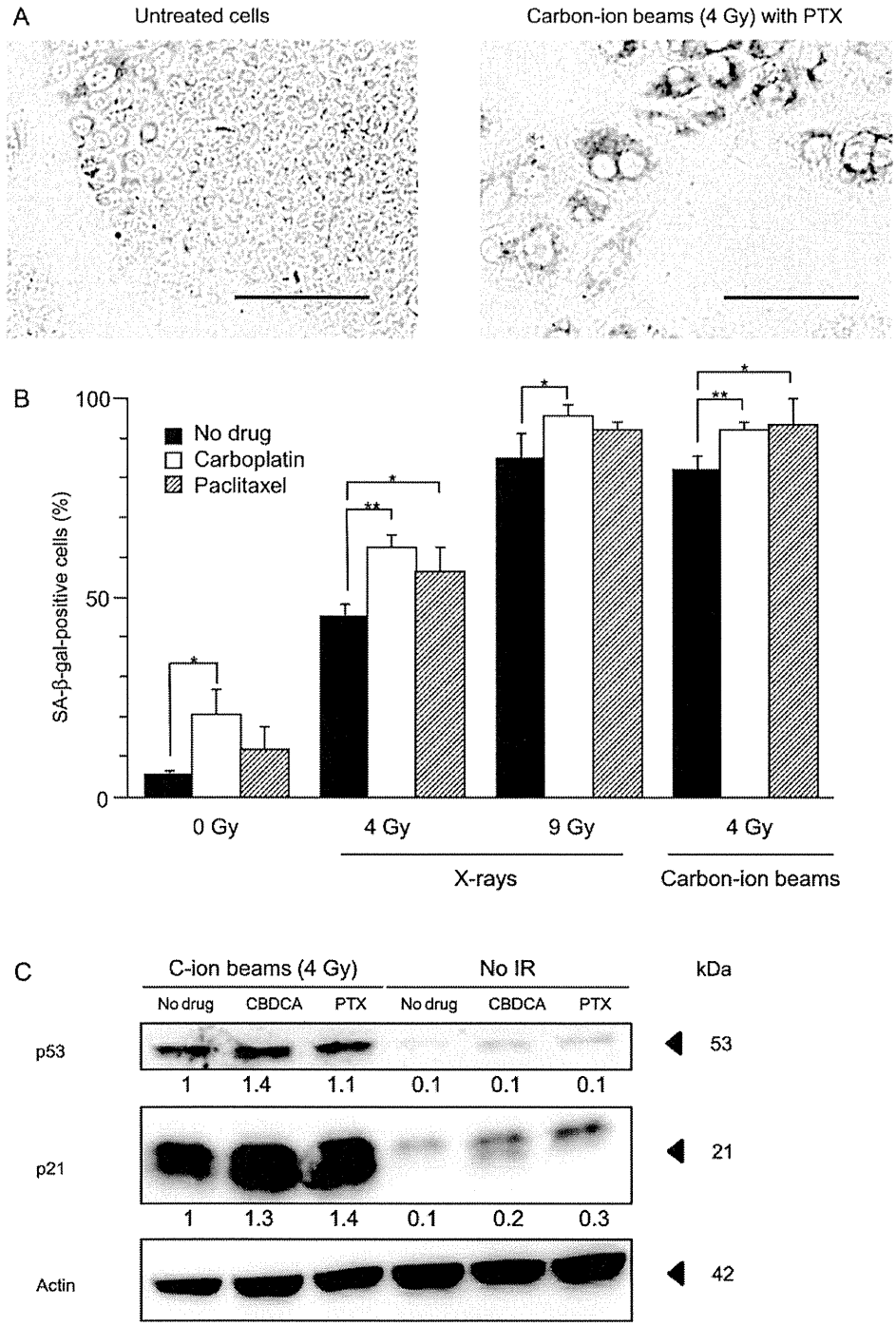

Fig. 5. Effects of carboplatin and paclitaxel on senescence induction in H460 cells irradiated with X-rays or carbon-ion beams. (**A**) Representative micrograph of cells negative (left panel) and positive (right panel) for SA-β-gal staining. Cells positive for SA-β-gal staining are shown in blue. Bars, 100 μm. (**B**) Percentages of SA-β-gal-positive cells. The mean ± SD is shown. A single asterisk indicates $P < 0.05$; two asterisks indicate $P < 0.01$. (**C**) Western blotting against p53 and p21. Actin was used as a loading control. Levels of p53 and p21 are shown as ratios to their levels in cells treated with carbon-ion beam irradiation alone, after normalization to loading controls. SA-β-gal staining was performed 3 days after irradiation. Carboplatin and paclitaxel were used at each respective IC_{50} (7.9 μM and 8.3 nM). C-ion = carbon-ion, CBDCA = carboplatin, PTX = paclitaxel, IR = irradiation.

(DDR) signaling is transduced from the generated DSBs to various downstream substrates via ataxia telangiectasia mutated (ATM) protein. Among the substrates of ATM, p53 plays a central role in inducing anti-tumor effects, including apoptotic cell death and senescence [23]. Meanwhile, carboplatin is known to sensitize cells to X-rays by enhancing the generation of DSBs [24] and persistent single-strand breaks (SSBs) [25], which can progress to DSBs through replication fork collapse in the S phase. In the present study, carboplatin enhanced the expression of p53 (Fig. 5C) and the induction of apoptosis (Fig. 4B and C) and senescence (Fig. 5B and C) in response to carbon-ion beam irradiation. Taken together, these results suggest that carboplatin sensitizes cells to carbon-ion beam irradiation by enhancing the generation of DSBs and consequently activating the DSBs–ATM–p53 axis. Evidence that carboplatin might exert its radiosensitizing effect via the DSB–ATM–p53 axis by enhancing radiation-induced DSBs, combined with our data showing that apoptosis and senescence induced by irradiation alone were comparable between X-rays and carbon-ion beams at their respective iso-survival doses, may provide a rationale for the observation that carboplatin had a similar effect on apoptosis and senescence induced by either beam source (Figs 4B and C, and 5B and C).

Nevertheless, the mechanisms underlying the observation that X-rays and carbon-ion beams had a similar effect on apoptosis and senescence at their iso-survival doses are largely unknown because the characteristics of the DDR after carbon-ion beam irradiation have not been well elucidated. The difficulty in investigating the DDR in carbon-ion beam irradiation is partially due to the complexity of the DNA damage generated by carbon-ion beams. It is thought that high-LET carbon-ion beams generate 'clustered DNA damage' characterized by a complex DNA lesion consisting of multiple DSBs and/or other forms of DNA damage, such as SSBs and base damage [26]. To date, efforts to identify the specific forms of DNA damage present in a lesion using molecular markers have been limited. For example, there is controversy as to whether a single molecule of γH2AX (a marker for DNA DSBs) corresponds to a single DSB generated by carbon-ion beam irradiation or whether it reflects a cluster of DSBs in close proximity. Recently, high-resolution imaging technology has emerged, with which a single molecule involved in DDR, such as Ku, can be detected [27]. We are currently preparing for the examination of the DDR in NSCLC cells using this high-resolution imaging technology. Furthermore, recent reports indicate that indirect action plays a role in cell killing in high-LET radiation (including carbon-ion beams), where direct action had hitherto been thought to be predominant [28, 29]. The similar phenotype in the induction of apoptosis and senescence between X-ray and carbon-ion beams observed in the present study should be further pursued in light of these findings.

In contrast to carboplatin, the mechanisms underlying the radiosensitizing effect of paclitaxel are not well understood, even with respect to X-ray irradiation. Accumulation of cells in the G2/M phase, which is highly radiosensitive, has been proposed as a candidate mechanism for the ability of paclitaxel to sensitize cells to X-rays [30]; however, this hypothesis remains controversial [31, 32]. Meanwhile, previous studies have demonstrated that high-LET beam irradiation has anti-tumor effects regardless of the cell cycle phase [33], indicating that paclitaxel may sensitize cells to carbon-ion beam irradiation through mechanisms other than G2/M arrest. Further research on the mechanisms through which paclitaxel sensitizes cells to carbon-ion beam irradiation is warranted.

The present study indicated that the radiosensitizing effect of carboplatin and paclitaxel to carbon-ion beams is comparable to the radiosensitizing effect of carboplatin and paclitaxel to X-rays at their respective iso-survival doses. It is noteworthy that carbon-ion beam radiotherapy can achieve highly conformal dose distribution (i.e. a high dose delivered to tumors while maintaining a tolerable dose in the surrounding normal tissue) compared with X-rays. These results suggest that the combination of carboplatin or paclitaxel with carbon-ion beam radiotherapy would be more clinically beneficial than combination with X-ray radiotherapy, leading to enhanced efficacy of the local therapy at the primary disease site.

The present study has limitations. First, the radiosensitizing effects of carboplatin and paclitaxel were examined separately because of the difficulty in determining the optimal balance of the doses of the two drugs that shows maximal SER. However, the two drugs are used concomitantly as platinum-doublet chemotherapy with X-rays in the clinic [14, 15] and thus the radiosensitizing effect of combined carboplatin and paclitaxel should be investigated in the future for the clinical application of platinum-doublet chemotherapy in combination with carbon-ion radiotherapy. Secondly, in the present study, only apoptosis and senescence were examined as endpoints for the anti-tumor effect; however, there are modes of reproductive death other than apoptosis and senescence [34]. In fact, Jinno-Oue *et al.* reported that carbon-ion beam irradiation induced autophagy along with apoptosis and senescence in glioma-derived cell lines [35]. Autophagy induced by ionizing irradiation can result in both cell survival and cell death (autophagic survival and autophagic cell death, respectively) [34, 36, 37]; however, to date, there are no established molecular markers that can distinguish autophagic cell death from autophagic cell survival and, therefore, in the present study, we did not evaluate autophagy as the mode of reproductive death induced by irradiation. In addition, the present study showed that in the particular cell line H460, senescence was the predominant mode of reproductive death induced by the combined treatment, suggesting that autophagic cell death may not be a major mode of reproductive death underlying the radiosensitizing effect of carboplatin and paclitaxel. Nevertheless,

comprehensive research covering various modes of reproductive death including apoptosis, senescence, autophagy and necrosis should be conducted to fully elucidate the mechanisms underlying the radiosensitizing effect of carboplatin and paclitaxel. Lastly, the present study examined only one cell line and thus these results may not be generally applicable to human NSCLC. Further studies using multiple cell lines will be required to generalize the ability of carboplatin and paclitaxel to sensitize tumor NSCLC cells to carbon-ion beam irradiation.

In summary, the present study showed that carboplatin and paclitaxel sensitized NSCLC H460 cells to carbon-ion beam irradiation by enhancing irradiation-induced apoptosis and senescence. These findings are a first step in providing a biological basis for the clinical use of combined therapy with carboplatin and/or paclitaxel and carbon-ion beam radiotherapy, although further efforts should be made to elucidate the underlying mechanism of the radiosensitizing effect and to generalize these findings to multiple cell lines.

FUNDING

This work was supported by JSPS KAKENHI Grant Number 24591834. Funding to pay the Open Access publication charges for this article was provided by JSPS KAKENHI Grant Number 24591834.

REFERENCES

1. Furuse K, Fukuoka M, Kawahara M *et al.* Phase III study of concurrent versus sequential thoracic radiotherapy in combination with mitomycin, vindesin and cisplatin in unresectable stage III non- small-cell lung cancer. *J Clin Oncol* 1999;**17**:2692–9.
2. Yamamoto N, Nakagawa K, Nishimura Y *et al.* Phase III study comparing second- and third-generation regimens with concurrent thoracic radiotherapy in patients with unresectable stage III non-small-cell lung cancer: West Japan Thoracic Oncology Group WJTOG0105. *J Clin Oncol* 2010;**28**:3739–45.
3. Curran WJ, Paulus R, Langer CJ *et al.* Sequential vs. concurrent chemoradiation for stage III non-small cell lung cancer: randomized phase III trial RTOG 9410. *J Natl Cancer Inst* 2011;**103**:1452–60.
4. Sause W, Kolesar P, Taylor S *et al.* Final results of phase III trial in regionally advanced unresectable non-small cell lung cancer: Radiation Therapy Oncology Group, Eastern Cooperative Oncology Group, and Southwest Oncology Group. *Chest* 2000;**117**:358–64.
5. Cox JD. Are the results of RTOG 0617 mysterious? *Int J Radiat Oncol Biol Phys* 2012;**82**:1042–4.
6. Kanai T, Furusawa Y, Fukutsu K *et al.* Irradiation of mixed beam and design of spread-out Bragg peak for heavy-ion radiotherapy. Radiat Res 1997;**147**:78–85.
7. Miyamoto T, Baba M, Sugane T *et al.* Carbon ion radiotherapy for stage I non-small cell lung cancer using a regimen of four fractions during 1 week. *J Thorac Oncol* 2007;**2**:916–26.
8. Sugane T, Baba M, Imai R *et al.* Carbon ion radiotherapy for elderly patients 80 years and older with stage I non-small cell lung cancer. *Lung Cancer* 2009;**64**:45–50.
9. Kitabayashi H, Shimada H, Yamada S *et al.* Synergistic growth suppression induced in esophageal squamous cell carcinoma cells by combined treatment with docetaxel and heavy carbon-ion beam irradiation. *Oncol Rep* 2006;**15**:913–8.
10. Combs SE, Bohl J, Elsasser T *et al.* Radiobiological evaluation and correlation with the local effect model (LEM) of carbon ion radiation therapy and temozolomide in glioblastoma cell lines. *Int J Radiat Biol* 2009;**85**:126–37.
11. Schlaich F, Brons S, Haberer T *et al.* Comparison of the effects of photon versus carbon ion irradiation when combined with chemotherapy *in vitro*. *Radiat Oncol* 2013;**8**:260.
12. Kelland L. The resurgence of platinum-based cancer chemotherapy. *Nat Rev Cancer* 2007;**7**:573–84.
13. Kavallaris M. Microtubules and resistance to tubulin-binding agents. *Nat Rev Cancer* 2010;**10**:194–204.
14. Choy H, Safran H, Akerley W *et al.* Phase II trial of weekly paclitaxel and concurrent radiation therapy for locally advanced non-small cell lung cancer. *Clin Cancer Res* 1998;**4**:1931–6.
15. Carter DL, Garfield D, Hathorn J *et al.* A randomized phase III trial of combined paclitaxel, carboplatin, and radiation therapy followed by weekly paclitaxel or observation for patients with locally advanced inoperable non-small-cell lung cancer. *Clin Lung Cancer* 2012;**13**:205–13.
16. Dillman RO, Seagren SL, Propert KJ *et al.* A randomized trial of induction chemotherapy plus high-dose radiation versus radiation alone in stage III non-small-cell lung cancer. *N Engl J Med* 1990;**323**:940–5.
17. Ohno T, Kanai T, Yamada S *et al.* Carbon ion radiotherapy at the Gunma University Heavy Ion Medical Center: new facility set-up. *Cancers (Basel)* 2011;**3**:4046–60.
18. Tennant JR. Evaluation of the trypan blue technique for determination of cell viability. *Transplantation* 1964;**2**: 685–94.
19. Mazumder S, Plesca D, Almasan A. Caspase-3 activation is a critical determinant of genotoxic stress-induced apoptosis. *Methods Mol Biol* 2008;**414**:13–21.
20. Adams JM. The Bcl-2 protein family: arbiters of cell survival. *Science* 1998;**281**:1322–6.
21. Gewirtz DA, Holt SE, Elmore LW. Accelerated senescence: an emerging role in tumor cell response to chemotherapy and radiation. *Biochem Pharmacol* 2008;**76**:947–57.
22. Levine AJ. p53, the cellular gatekeeper for growth and division. *Cell* 1997;**88**:323–31.
23. Cremona CA, Behrens A. ATM signalling and cancer. *Oncogene* 2014;**33**:3351–60.
24. Yang LX, Douple EB, O'Hara JA *et al.* Production of DNA double-strand breaks by interactions between carboplatin and radiation: a potential mechanism for radiopotentiation. *Radiat Res* 1995;**143**:309–15.
25. Yang LX, Douple EB, O'Hara JA *et al.* Carboplatin enhances the production and persistence of radiation-induced DNA single-strand breaks. *Radiat Res* 1995;**143**:302–8.
26. Terato H, Ide H. Clustered DNA damage induced by heavy ion particles. *Biol Sci Space* 2004;**18**:206–15.

27. Britton S, Coates J, Jackson SP. A new method for high-resolution imaging of Ku foci to decipher mechanisms of DNA double-strand break repair. *J Cell Biol* 2013;**202**:579–95.
28. Ito A, Nakano H, Kusano Y *et al.* Contribution of indirect action to radiation-induced mammalian cell inactivation: dependence on photon energy and heavy-ion LET. *Radiat Res* 2006;**165**:703–12.
29. Hirayama R, Ito A, Tomita M *et al.* Contributions of direct and indirect actions in cell killing by high-LET radiations. *Radiat Res* 2009;**171**:212–8.
30. Tishler RB, Schiff PB, Geard CR *et al.* Taxol: a novel radiation sensitizer. *Int J Radiat Oncol Biol Phys* 1992;**22**:613–7.
31. Wenz F, Greiner S, Germa F *et al.* Radiochemotherapy with paclitaxel: synchronization effects and the role of p53. *Strahlenther Onkol* 1999;**175**:2–6.
32. Niero A, Emiliani E, Monti G *et al.* Paclitaxel and radiotherapy: sequence-dependent efficacy—a preclinical model. *Clin Cancer Res* 1999;**5**:2213–22.
33. Bird RP, Burki HJ. Survival of synchronized Chinese hamster cells exposed to radiation of different linear-energy transfer. *Int J Radiat Biol Relat Stud Phys Chem Med* 1975;**27**: 105–20.
34. Galluzzi L, Vitale I, Abrams JM *et al.* Molecular definitions of cell death subroutines: recommendations of the Nomenclature Committee on Cell Death 2012. *Cell Death Differ* 2012; **19**:107–20.
35. Jinno-Oue A, Shimizu N, Hamada N *et al.* Irradiation with carbon ion beams induces apoptosis, autophagy, and cellular senescence in a human glioma-derived cell line. *Int J Radiat Oncol Biol Phys* 2010;**76**:229–41.
36. White E. Deconvoluting the context-dependent role for autophagy in cancer. *Nat Rev Cancer* 2012;**12**:401–10.
37. Klionsky DJ, Abdalla FC, Abeliovich H *et al.* Guidelines for the use and interpretation of assays for monitoring autophagy. *Autophagy* 2012;**8**:445–544.

RADIATION ONCOLOGY

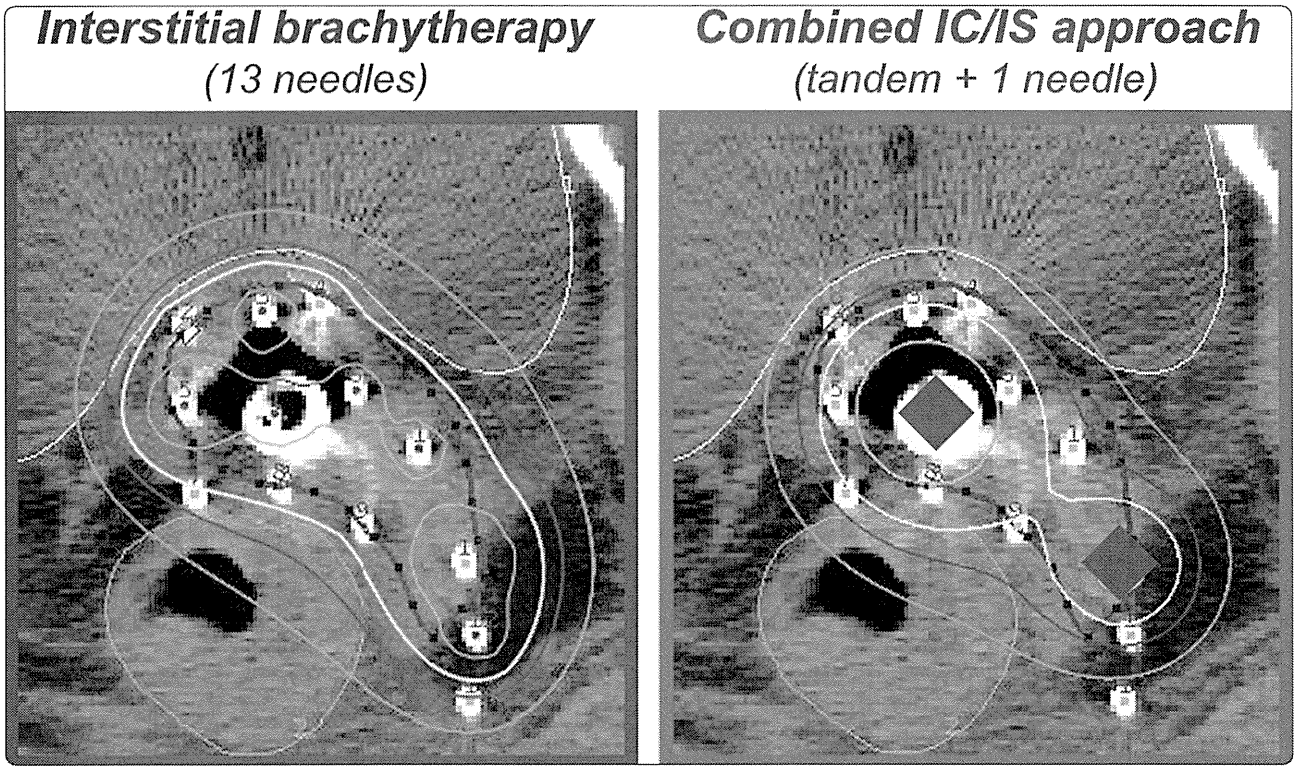

Can combined intracavitary/interstitial approach be an alternative to interstitial brachytherapy with the Martinez Universal Perineal Interstitial Template (MUPIT) in computed tomography-guided adaptive brachytherapy for bulky and/or irregularly shaped gynecological tumors?

Oike *et al.*

BioMed Central

Oike *et al. Radiation Oncology* 2014, **9**:222
http://www.ro-journal.com/content/9/1/222

Oike et al. Radiation Oncology 2014, 9:222
http://www.ro-journal.com/content/9/1/222

RADIATION ONCOLOGY

RESEARCH Open Access

Can combined intracavitary/interstitial approach be an alternative to interstitial brachytherapy with the Martinez Universal Perineal Interstitial Template (MUPIT) in computed tomography-guided adaptive brachytherapy for bulky and/or irregularly shaped gynecological tumors?

Takahiro Oike*, Tatsuya Ohno, Shin-ei Noda, Hiroki Kiyohara, Ken Ando, Kei Shibuya, Tomoaki Tamaki, Yosuke Takakusagi, Hiro Sato and Takashi Nakano

Abstract

Background: Interstitial brachytherapy (ISBT) is an optional treatment for locally advanced gynecological tumours for which conventional intracavitary brachytherapy (ICBT) would result in suboptimal dose coverage. However, ISBT with Martinez Universal Perineal Interstitial Template (MUPIT), in which ~10-20 needles are usually applied, is more time-consuming and labor-intensive than ICBT alone, making it a burden on both practitioners and patients. Therefore, here we investigated the applicability of a combined intracavitary/interstitial (IC/IS) approach in image-guided adaptive brachytherapy for bulky and/or irregularly shaped gynecological tumours for which interstitial brachytherapy (ISBT) was performed.

Methods: Twenty-one consecutive patients with gynecological malignancies treated with computed tomography-guided ISBT using MUPIT were analyzed as cases for this dosimetric study. For each patient, the IC/IS plan using a tandem and 1 or 2 interstitial needles, which was modeled after the combined IC/IS approach, was generated and compared with the IS plan based on the clinical ISBT plan, while the IC plan using only the tandem was applied as a simplified control. Maximal dose was prescribed to the high-risk clinical target volume (HR-CTV) while keeping the dose constraints of D_{2cc} bladder < 7.0 Gy and D_{2cc} rectum < 6.0 Gy. The plan with D90 HR-CTV exceeding 6.0 Gy was considered acceptable.

Results: The average D90 HR-CTV was 77%, 118% and 140% in the IC, IC/IS and IS plans, respectively, where 6 Gy corresponds to 100%. The average of the ratio of D90 HR-CTV to D_{2cc} rectum (gain factor (GF) $_{rectum}$) in the IC, IC/IS and IS plans was 0.8, 1.3 and 1.5 respectively, while $GF_{bladder}$ was 0.9, 1.4 and 1.6, respectively. In the IC/IS plan, D90 HR-CTV, GF_{rectum} and $GF_{bladder}$ exceeded 100%, 1.0 and 1.0, respectively, in all patients.

Conclusions: These data demonstrated that the combined IC/IS approach could be a viable alternative to ISBT for gynecological malignancies with bulky and/or irregularly shaped tumours.

* Correspondence: oiketakahiro@gmail.com
Department of Radiation Oncology, Gunma University Graduate School of Medicine, 3-39-22, Showa-machi, Maebashi, Gunma 371-8511, Japan

Background

Interstitial brachytherapy (ISBT) is a choice of curative treatment for locally advanced gynecological tumours with extension to the lateral parametria and/or lower vaginal wall, for which intracavitary brachytherapy (ICBT) would result in suboptimal dose coverage [1]. Accordingly, we have been treating patients with locally advanced cervical tumours and other gynecological malignancies using in-room and in-situ computed tomography (CT)-guided adaptive high dose rate (HDR) ISBT with Martinez Universal Perineal Interstitial Template (MUPIT, Nucleotron) [2]. However, ISBT with MUPIT, in which ~10-20 needles are usually applied, is more time-consuming and labor-intensive than ICBT alone, making it a burden on practitioners. Moreover, patients receiving this treatment also must bear the hardship of keeping interstitial needles implanted for several days. Besides, facilities at which ISBT is routinely performed are limited in Japan [3]. These aspects have prompted us to explore alternative treatment strategies for bulky and/or irregularly shaped tumours.

The recent development of technologies in image-guided adaptive brachytherapy (IGABT) has enabled the integration of magnetic resonance imaging (MRI) or CT images into the treatment planning process [4-6]. This has resulted in the adaptive target concept, with dose volume assessment balancing constraints for the clinical target volume (CTV) and organs at risk (OARs). In 2011, Pötter *et al.* reported the long-term results of 156 cervical cancer patients treated with chemoradiotherapy, demonstrating an overall 3-year local control rate of 92% for locally advanced tumours (>5 cm) treated with the MRI-guided combined intracavitary/interstitial (IC/IS) approach [7]. This indicates that the image-guided combined IC/IS approach with a few interstitial needles could be a viable alternative to ISBT with MUPIT in the treatment of bulky and/or irregularly shaped tumours. Therefore, here we performed a dosimetric study to explore the applicability of the CT-guided combined IC/IS approach in patients with gynecological malignancies with bulky and/or irregularly shaped tumours, who were actually treated with CT-guided ISBT with MUPIT.

Methods

Twenty-one consecutive patients with gynecological malignancies treated with CT-guided adaptive HDR ISBT with MUPIT using iridium-192 source at Gunma University Hospital between April 2008 and February 2013 were selected by IRB-approved retrospective chart review. Fourteen of them (67%) were cervical cancer patients. The rest included vaginal cancer (3 patients), uterine endometrioid cancer (3 patients) and ovarian cancer (1 patient). Among them, 10/14, 1/3, 3/3 and 1/1 patients with cervical, vaginal, uterine endometrioid and ovarian cancer had recurrent tumours. Although these cases were heterogeneous in terms of primary tumour site and whether they were primary diseases or recurrences, they had the commonality of developing bulky and/or irregularly shaped tumours in the uterine cervix or vaginal stump and/or parametrium. Hence, they were considered to be favorable hypothetical cases of locally advanced cervical cancer, which has the indication for the IC/IS approach in the clinic. For example, a recurrent ovarian cancer case showed an intrapelvic tumour with bilateral parametrial involvement predominantly in the right side (Additional file 1: Figure S1). Average ± standard deviation (SD) of high-risk CTV (HR-CTV) in the present study was 60 ± 32 cm^3, which was similar to the values of patients with locally advanced cervical cancer treated with combined IC/IS by the Utrecht group (66 ± 34 cm^3) [8]. Moreover, in our study, the distance between the tandem and the outer contour of HR-CTV was 30 mm or greater in all cases. The Utrecht group employed a distance of 30 mm as cutoff value for adding interstitial needles to the usual applicator consisting of the tandem and ovoids in IGABT for locally advanced cervical cancer [9]. Accordingly, the Vienna group reported that a distance of 25 mm in the plane of point A and that of 35 mm at ring level could be covered by sufficient dose using only the intracavitary part of the Vienna applicator [10]. Together, these data suggest that the cases selected in the current study were typical of extended tumours for which ISBT is recommended.

Application of the tandem, an endovaginal cylinder with MUPIT and interstitial needles was performed under in-room and in-situ CT guidance. Detailed procedure of the actually performed ISBT was previously described [2]. Target delineation was performed on CT images taken by an in-room CT scanner with reference to MRI images taken just before brachytherapy. The contours of HR-CTV, rectum and bladder were delineated according to the GEC-ESTRO recommendations [4].

We aimed to assess the applicability of a plan using the tandem and a few interstitial needles (IC/IS plan) as a viable alternative to the actually performed ISBT plan using MUPIT (IS plan). For this purpose, the IC/IS plan was generated on the CT image used for the actual ISBT treatments in each patient using the PLATO Brachytherapy Planning System (ver.14.3.6, Nucletron) or Oncentra (ver.4, Nucletron). For the IC/IS plan, the number of interstitial needles used for source loading was set at 1 or 2, taking the burden of needle application for the practitioners into consideration. Interstitial needles located at the edge of the extended part of HR-CTV were selected from needles implanted with MUPIT (9–18 needles; median, 14) based on visual inspection. One needle was used in 17 cases with unilaterally extended tumours, while 2 needles were selected in 4 cases with

bilaterally extended tumours. Needles implanted in laterodorsal positions were most frequently selected (Figure 1), consistent with a previous report showing 95% of locally advanced cervical cancer cases treated with the Utrecht applicator received needle implantation in laterodorsal positions [8]. This suggests the authenticity of the positions of the needles selected in the current study as those used for the combined IC/IS approach. The IC plans, with only the tandem used for source loading, were generated as simplified controls since treatment plans with ovoids or a ring applicator with a tandem have large diversity in the spatial disposition of the applicators.

In the treatment planning for each of the IC, IC/IS and IS plans, the highest possible dose was prescribed to HR-CTV while keeping the dose constraints for rectum and bladder. Comparison of dose volume parameters for HR-CTV between the plans while keeping the same dose constraints for the OARs helps clarify the dosimetric gain of the plans. We have previously investigated late rectal complications in cervical cancer patients treated with EBRT plus ICBT, showing that the average total EQD2 ($\alpha/\beta = 3.0$) for D_{2cc} rectum in cases with late rectal complications and those without was 69 and 57 Gy, respectively. Based on these findings, here we set the dose constraint for rectum at $D_{2cc} < 6$ Gy, which results in total EQD2 of 59 Gy when the Japanese standard treatment regimen for advanced cervical cancer (30 Gy/15 fractions of whole pelvic irradiation followed by 20 Gy/10 fractions of EBRT with midline block and 4 sessions of ICBT) was employed [11]. There has been no concrete evidence so far regarding the dose constraint for bladder using the Japanese treatment regimen. However, several European groups have revealed that the tolerability of bladder to radiotherapy is relatively higher than that of rectum [7,8]. In reference to their data, we set the dose constraint for bladder at $D_{2cc} < 7$ Gy.

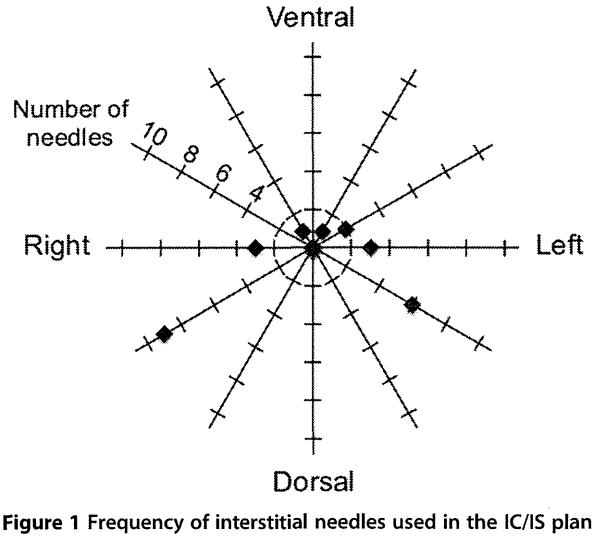

Figure 1 Frequency of interstitial needles used in the IC/IS plan per needle location. Relative locations of the needles to the tandem in a transverse plane were plotted in steps of 30 degrees. Twenty-five needles in 21 patients were used.

D90, the most significant dose volume parameter for local control in IGABT for cervical cancer [12], was used to assess HR-CTV coverage. We previously reported DVH analysis of ICBT for cervical cancer, in which CT images taken just before ICBT were superimposed on the 3-dimensional treatment plan of ICBT [13]. The study demonstrated that 'tumour volumes' almost corresponding to the current HR-CTV in GEC-ESTRO recommendations [5] receiving less than a total of 24 Gy in 4 fractions were significantly larger in patients with local recurrence than in those with local control. Based on these data, here, a plan showing D90 HR-CTV higher than 6 Gy while keeping the dose constraints for the OARs was considered acceptable.

To clearly understand the dosimetric gain of a plan, gain factor (GF) was defined as the ratio of D90 HR-CTV to D_{2cc} of rectum and bladder, respectively: GF_{rectum} = D90 HR-CTV/D_{2cc} rectum, $GF_{bladder}$ = (D90 HR-CTV/D_{2cc} bladder) × 7/6. In the present study, 6 Gy for D_{2cc} rectum and 7 Gy for D_{2cc} bladder were employed as dose constraints, and the plan showing D90 HR-CTV higher than 6 Gy while keeping these dose constraints was considered acceptable. Hence, with regard to rectum, GF_{rectum} of a "borderline-acceptable" plan showing D90 HR-CTV of 6 Gy and D_{2cc} rectum of 6 Gy becomes 1.0, favorably. However, in the case of bladder, $GF_{bladder}$ of a "borderline-acceptable" plan showing D90 HR-CTV of 6 Gy and D_{2cc} bladder of 7 Gy becomes 0.86 (i.e., 6/7). In order to make this value 1.0, the coefficient "7/6" was used in calculating $GF_{bladder}$. Together, a GF higher than 1.0 indicates that the plan has the potential of being definitive and acceptable in terms of late toxicities for rectum or bladder. The treatment plans were confirmed by two radiation oncologists (T. Oike and T. Ohno).

D98 and V_{6Gy} of HR-CTV were also analyzed for target coverage, while V_{12Gy} HR-CTV was examined for high dose volume [5]. For inter-comparison of plans with different dose prescriptions, V_{6Gy} and V_{12Gy}, the volumes receiving at least 6 and 12 Gy, were selected as alternatives for V100 and V200, respectively. Differences in DVH parameters were evaluated for significance by paired *t*-test using StatMateIII (ver. 3.17, ATMS). A P value < 0.05 was considered significant.

Of note, in the present study, the cases were analyzed simply as samples for dosimetric comparison of the treatment plans to test the applicability of the combined IC/IS approach for bulky and/or irregularly shaped tumours. Thus, here we do not aim to discuss the curability of these cases in light of the actually performed treatments. Accordingly, the clinical information, including treatment

history, simultaneous use of EBRT and total EQD2, is not presented.

Results and discussion

The IC plans with only the tandem resulted in insufficient HR-CTV coverage as expected (Figure 2a-e, Figure 3a, Table 1). D90 HR-CTV was below 100% (i.e., 6.0 Gy) in 81% (17/21). GF_{rectum} and $GF_{bladder}$ were below 1.0 in 81% (17/21) and 52% (11/21), respectively. Interestingly, the addition of one or two needles to the IC plan (i.e., the IC/IS plan) dramatically improved the HR-CTV coverage (Figure 2a-e, Figure 3b, Table 1). The D90 HR-CTV, GF_{rectum}, $GF_{bladder}$, D98 HR-CTV and V_{6Gy} HR-CTV of the IC/IS plan was significantly higher than that of the IC plan ($P < 0.001$ in all parameters). Of note, D90 HR-CTV, GF_{rectum} and $GF_{bladder}$ exceeded 100% (i.e., 6.0 Gy), 1.0 and 1.0, respectively, in all cases. These data indicate that the combined IC/IS approach can achieve satisfactory dose distribution with acceptable HR-CTV coverage and tolerable sparing of rectum and bladder in bulky and/or irregularly shaped tumours for which ISBT was performed.

In our IC/IS model with a few needles, the reproducible placement of needles to the most appropriate positions of HR-CTV is required to achieve favorable dose distribution. For this purpose, the Vienna (I) and Utrecht applicators dedicated to the combined IC/IS approach would become effective tools [10,14], although the lateral dimensions of the extended isodose lines are limited after adding needles. Furthermore, exploration to identify the optimal treatment plan (i.e., optimal number and position of needles) for balancing satisfactory dose distributions and clinical burden should be conducted in the near future.

Our data and those of others indicate that needles in laterodorsal positions are most frequently used for source loading in the combined IC/IS approach (Figure 1) [8]. Meanwhile, laterodorsal contours of HR-CTV tend to be overestimated by CT compared with MRI, which is a major advantage of MRI in discrimination of tumours and adjacent normal tissue [5,15]. In this regard, it can be said that our study has a limitation in comparing the target coverage in the laterodorsal directions between ISBT with MUPIT and the combined IC/IS approach. Thus, an analysis in the same way as the present study and using MRI-based treatment plans should be carried out. Thus, to validate our results of the MRI-guided combined IC/IS approach, we are preparing to introduce a treatment planning system in

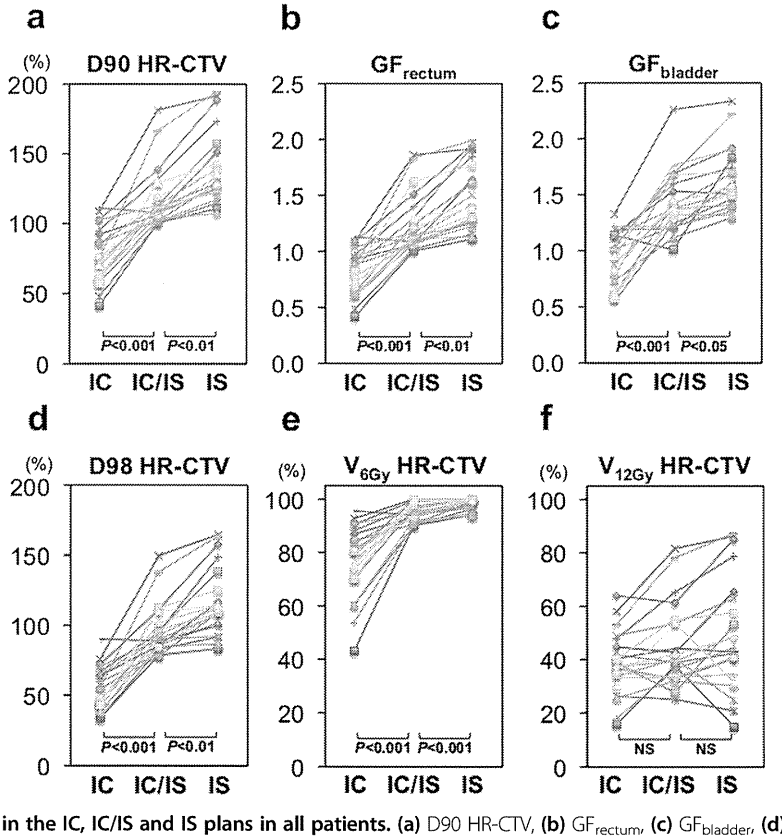

Figure 2 DVH parameters in the IC, IC/IS and IS plans in all patients. (a) D90 HR-CTV, **(b)** GF_{rectum}, **(c)** $GF_{bladder}$, **(d)** D98 HR-CTV, **(e)** V_{6Gy} HR-CTV, **(f)** V_{12Gy} HR-CTV. D90 and D98 HR-CTV were described in "%", where 6 Gy corresponds to 100%. NS, not statistically significant.